SPECIAL
DIMES
COLLECTION

Float-Derived Isopycnal Diffusivities in the DIMES Experiment

J. H. LaCasce

University of Oslo, Oslo, Norway

R. Ferrari, J. Marshall, and R. Tulloch

Massachusetts Institute of Technology, Cambridge, Massachusetts

D. Balwada and K. Speer

The Florida State University, Tallahassee, Florida

ABSTRACT

As part of the Diapycnal and Isopycnal Mixing Experiment in the Southern Ocean (DIMES), 210 sub-surface floats were deployed west of the Drake Passage on two targeted density surfaces. Absolute (single particle) diffusivities are calculated for the floats. The focus is on the meridional component, which is less affected by the mean shear. The diffusivities are estimated in several ways, including a novel method based on the probability density function of the meridional displacements. This allows the determination of the range of possible lateral diffusivities, as well as the period over which the spreading can be said to be diffusive. The method is applied to the float data and to synthetic trajectories generated with the Massachusetts Institute of Technology General Circulation Model (MITgcm). Because of ballasting problems, many of the floats did not remain on their targeted density surface. However, the float temperature records suggest that most occupied a small range of densities, so the floats were grouped together for the analysis. The latter focuses on a subset of 109 of the floats, launched near 105°W. The different methods yield a consistent estimate for the diffusivity of $800 \pm 200 \, \mathrm{m^2 \, s^{-1}}$. The same calculations were made with model particles deployed on 20 different density surfaces and the result for the particles deployed on the neutral density surface $\gamma = 27.7$ surface was the same within the errors. The model was then used to map the variation of the diffusivity in the vertical, near the core of the Antarctic Circumpolar Current (ACC). The results suggest mixing is intensified at middepths, between 1500 and 2000 m, consistent with several previous studies.

1. Introduction

The goal of the Diapycnal and Isopycnal Mixing Experiment in the Southern Ocean (DIMES) was to measure isopycnal and vertical diffusivities in the region west and east of the Drake Passage. The vertical diffusivity results, based on microstructure and tracer measurements, were discussed by Ledwell et al. (2011) and St. Laurent et al. (2012). The isopycnal dispersion was measured using both the tracer and floats. The present paper concerns the latter. The tracer dispersion is described in a companion paper (Tulloch et al. 2013, manuscript submitted to *J. Phys. Oceanogr.*), and additional float statistics and circulation results are presented by D. Balwada et al. (2013, unpublished manuscript).

Float dispersion can be quantified in several ways. One is descriptive (where the floats go, how they spread, whether they follow topography, etc.). Examples include Swallow's landmark studies of the deep flow in the North Atlantic (Swallow and Worthington 1957; Swallow 1971). D. Balwada et al. (2013, unpublished manuscript) give such a descriptive view of the float dispersion in DIMES, including the influence of topography. The second approach concerns how Lagrangian (particle) dispersion is affected by coherent structures, such as manifolds (e.g., Haller and Yuan 2000; Wiggins 2005). Such studies are usually made with modeled or reconstructed flows with

Corresponding author address: Joe LaCasce, Department of Geosciences, University of Oslo, P.O. Box 1022 Blindern, 0315 Oslo, Norway.
E-mail: j.h.lacasce@geo.uio.no

synthetic particles; the application to in situ data is still in its infancy. Third, there is the statistical description of dispersion (Freeland et al. 1975; Owens 1991; Davis 1991; LaCasce 2008), which remains the most commonly used method for studying oceanic data. This is the approach used here.

Dispersion statistics in turn can be divided into two types: those of single particles (absolute dispersion) and those of groups of particles (relative dispersion) (Bennett 2006; LaCasce 2008). The DIMES floats were deployed in clusters, precisely to study relative dispersion; those results will be described in a subsequent paper. Here, we focus on absolute dispersion and in particular on the isopycnal diffusivity. The latter is central in characterizing tracer spreading (Davis 1991; Ledwell et al. 1998) and can also be used for parameterizing subgrid-scale mixing in coarse-resolution models (Plumb and Mahlman 1987; Griffies 2004).

Previous in situ measurements of the lateral diffusivity in the Southern Ocean derive primarily from surface drifters (Zhurbas and Oh 2003; Rupolo 2007; Lumpkin and Pazos 2007; Sallée et al. 2008). These analyses suggest large regional variations. In the boundary currents (in the Agulhas and Brazil Currents and near the Kerguelen and Campbell Plateaus), diffusivities can reach values of $10^4 \, \mathrm{m^2 \, s^{-1}}$. In more quiescent regions, the diffusivities can be two orders of magnitude smaller. The DIMES floats were deployed in one such region (although they later entered the Drake Passage where they experienced much more rapid spreading).

The dispersion in the Southern Ocean is also strongly anisotropic because of the influence of the Antarctic Circumpolar Current (ACC). Diffusivity estimates in the direction parallel to the current typically exceed those in the perpendicular direction (section 4a). Determining along-stream diffusivities requires removing the mean contribution, usually by averaging drifter velocities in geographical bins; the diffusivities are then calculated from the residuals (Davis 1991). However, a perfect mapping of the mean is essentially impossible, implying the mean will always contribute to the along-stream dispersion. Thus, the anisotropy remains, as with shear dispersion (Young and Jones 1991).

An alternate approach is to focus exclusively on the cross-stream dispersion. It is this component that is also of interest in the broader climate perspective, as this mediates tracer exchange between the subtropics and southern polar regions. In the DIMES deployment region, the cross-stream component is essentially the meridional one because the ACC is nearly zonal here (section 4a). However, recent studies demonstrate that the mean flow also affects the cross-stream diffusivity by suppressing mixing (Green 1970; Marshall et al. 2006;

Ferrari and Nikurashin 2010; Sallée et al. 2011; Klocker et al. 2012a). Neglecting this effect results in overly large estimates of the diffusivity. This may help explain the large values noted above, as boundary currents are by definition dominated by mean flows.

In line with this, diffusivities derived from synthetic tracer, which solely reflect cross-stream mixing, are typically lower. Using a synthetic tracer advected by an altimetric velocity, for example, Marshall et al. (2006) obtained diffusivities in the DIMES region on the order of $10^3 \, \mathrm{m^2 \, s^{-1}}$, somewhat less than previously estimated from drifters. This raised doubts as to whether one can measure diffusivities from particles in such cases. But Klocker et al. (2012a) demonstrated that tracer- and particle-based estimates agree, as long as the diffusivities are calculated over sufficiently long times (and as long as there is sufficient data).

Subsurface diffusivity estimates in the Southern Ocean are sorely lacking. Most Lagrangian data come from Argo floats that do not lend themselves to diffusivity calculations due to their large vertical excursions (for positional fixes at the surface) and coarse temporal resolution. Existing estimates derive primarily from models, both from synthetic tracer (Smith and Marshall 2009; Abernathey et al. 2010) and particles (Klocker et al. 2012b). These suggest, interestingly, that mixing is intensified below the surface in the vicinity of a critical level (where the mean flow speed matches the eddy propagation speed). An additional goal of DIMES was to detect such a subsurface maximum.

Hereafter, we calculate diffusivities using the DIMES floats. As learned from the aforementioned studies, the calculation itself can be a delicate matter. This is particularly true with sparse in situ data. Furthermore, there are several different approaches currently in use, and these can give different results. From Taylor (1921), we know that dispersion grows ballistically in time initially and is diffusive only after several Lagrangian integral times, but few studies test when the dispersion is actually diffusive.

In section 2, we briefly describe the float data and also a set of synthetic particle trajectories used for comparison. In section 3, we discuss how the diffusivities are calculated and propose a new method that allows testing when the spreading is diffusive. Results are given in section 4 for both the synthetic particles and the DIMES floats. The diffusivities in the model agree within the errors with those derived from floats. The section includes a calculation of the diffusivity with depth, using the synthetic particles.

2. Data and model

In DIMES, 128 acoustically tracked RAFOS floats were deployed on the $\gamma = 27.9$ neutral density surface
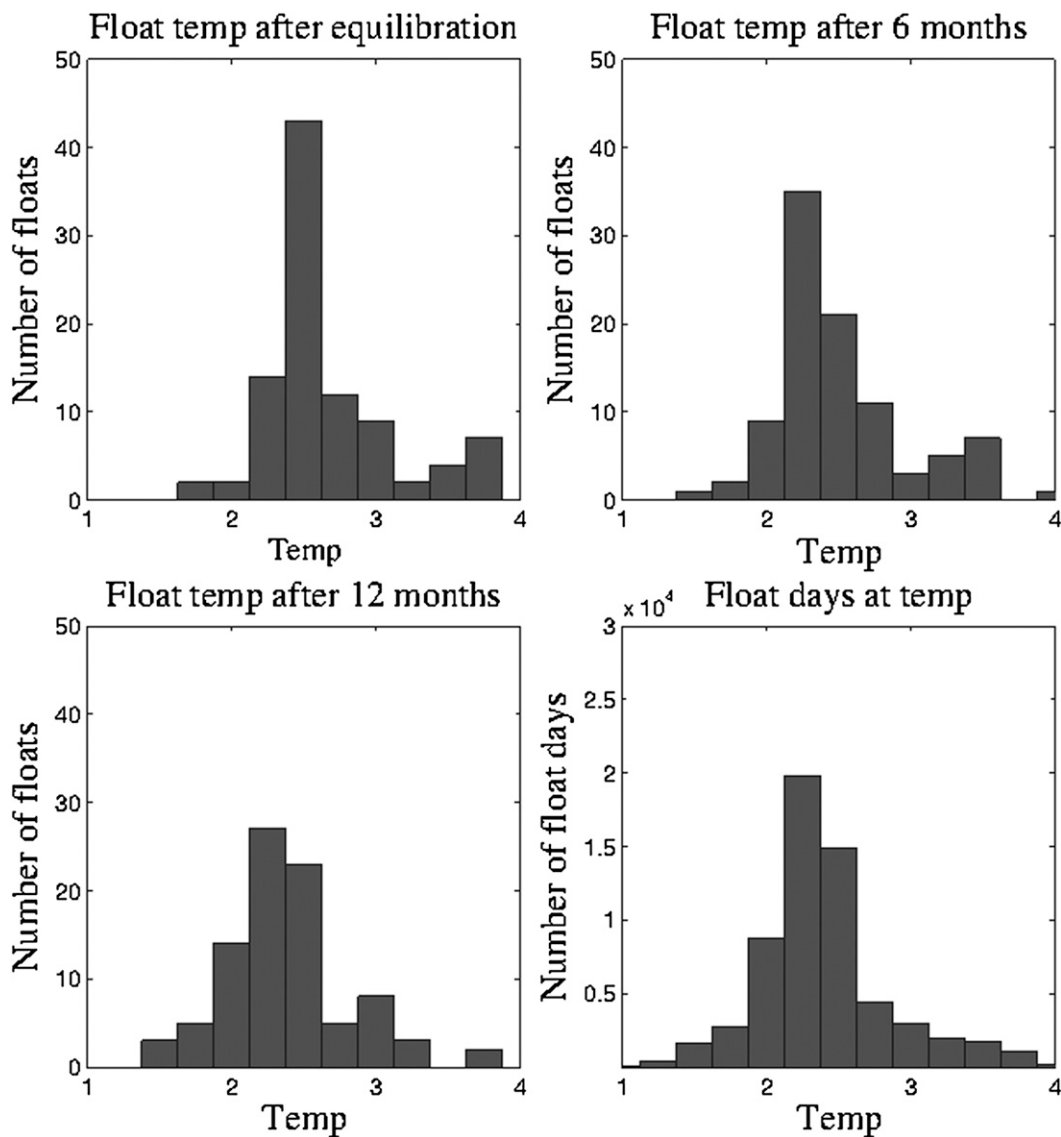
FIG. 1. Histograms of float temperature (top left) at deployment, (top right) after 6 months, and (bottom left) after 12 months. (bottom right) A histogram of the number of float days as a function of temperature. The first three histograms indicate the floats are shifting in time to colder temperatures, while the float day histogram shows the majority are clustered around 2.3°C.

near 1500-m depth. An additional 82 floats were deployed on the $\gamma = 27.6$ neutral density surface near 700-m depth. The floats were designed to follow isopycnal surfaces, but unfortunately a number experienced problems with their compressibility apparatus, causing some to surface prematurely and others to sink during their missions.

This can be inferred from Fig. 1, which shows histograms of float temperature at deployment and after 6 and 12 months. Note that the floats do not measure density but temperature. At deployment, the distribution is peaked at 2.5°C, with a secondary peak near 3.5°C. At 6 months both peaks are present, but the primary peak has shifted to colder

temperatures and is broader. The trend continues at 12 months and the warmer peak has essentially disappeared. This is consistent with a downward shift in the floats.

Shown in Fig. 1 (bottom right) is the total number of float days for each temperature class. While there are outliers, the majority of the floats are in the 2°–2.6°C range, with a peak near 2.3°C. Temperature is well correlated with density in this region at the depth of the floats. Comparing temperatures and densities in the Southern Ocean State Estimate (SOSE), we find that 2.3°C corresponds to a neutral density in the range $\gamma = 27.7–27.9$. Thus, we take all floats together for the analysis

and assume they are representative of this density range. Further details about the float behavior are given by D. Balwada et al. (2013, unpublished manuscript).

Together, we have 135 float trajectories of usable quality. We will focus on a subset of these (109 floats) that was launched farthest to the west (between 60° and 55°S, and near 105°W). The remaining floats were launched nearer the Drake Passage and exited the western region much sooner. The trajectories of the 109 floats are shown in Fig. 3 (top; described in greater detail below). As a group, they migrate eastward and slightly southward approaching the Drake Passage. A number also exhibit distinct meandering motion initially. When the floats reach the Drake Passage, they converge and then turn northeast. The meridional dispersion thereafter is dominated by the mean flow and is substantially greater than that to the west.

The synthetic trajectories were generated with a regional version of the Massachusetts Institute of Technology General Circulation Model (MITgcm) (Marshall et al. 1997). The model domain includes the Drake Passage, running from 75° to 35°S and from 160° to 20°W, and has a horizontal resolution of 1/20° (3 km × 6 km) in the DIMES region. The model has 100 layers of unequal thickness such that the top 70 layers, which span the upper 1900 m, are all less than 35 m thick. For further details on model forcing and initial conditions, see Tulloch et al. (2013, manuscript submitted to *J. Phys. Oceanogr.*). Particles were released where the selected DIMES floats were released every 10 days during the 2-yr simulation and on 20 different γ surfaces. Additional sets of particles were released at 60°S, between 110° and 100°W, for additional calculations (section 4b).

We then had to choose which set of particles to compare with the floats (as the latter span a range of densities). To do this, we compared the mean longitudinal drifts of each of the 20 sets of particles with those of the floats. The particles deployed on the $\gamma = 27.7$ surface (at 910 m initially) exhibited nearly the same drift (see below). So we used these for calculating diffusivities.

An obvious advantage of the model is that it permits having many more particles. Taking all the 10-day launches together, we obtain a set of 600. Having many more trajectories is of course possible, but this number was sufficient for the subsequent comparisons. The model trajectories span a larger region than do the floats, both upstream and downstream of the Drake Passage (Fig. 3, bottom; described in greater detail below). Nevertheless, the results from the two sets are very similar.

3. Methods

The calculation of lateral (eddy) diffusivities from Lagrangian data dates back to Taylor (1921). Davis (1991) extended Taylor's formalism to inhomogeneous ocean flows. The lateral diffusivity is now the most common statistic calculated with Lagrangian data after the mean velocity and variance fields (e.g., LaCasce 2008).

The diffusivity, for example, in the meridional direction, is defined as

$$\kappa_y(t) \equiv \frac{1}{2}\frac{d}{dt}\langle [y(t) - y_0]^2 \rangle, \tag{1}$$

$$= \langle v(t)(y - y_0) \rangle, \tag{2}$$

$$= \left\langle v(t)\int_0^t v(t')\,dt' \right\rangle, \tag{3}$$

$$= \int_0^t \langle v(t)v(t') \rangle\,dt', \tag{4}$$

$$= \nu^2 \int_0^t R(t')\,dt', \quad \text{and} \tag{5}$$

$$\equiv \nu^2 T_L. \tag{6}$$

In (1), the diffusivity is equal to one-half the derivative of the dispersion, the mean square displacement from the starting latitude y_0. The angle brackets indicate an ensemble average, generally taken to be an average over particles released in a given region or experiment. In (2), the time derivative is moved through the brackets, demonstrating that the diffusivity is also equal to the correlation between the particle velocity and its displacement. In (3), the displacement is replaced by the temporal integral of the velocity. If the flow is homogeneous, we can drop any reference to location (as is done here). Then the diffusivity is the integral of the velocity autocorrelation in (4). If the velocity statistics are also stationary, the autocorrelation can be normalized by factoring out ν^2 in (5), the velocity variance. The resulting integral yields the Lagrangian time scale T_L in (6). For diffusive flows, T_L and κ_y asymptote to constant values as the upper integrand t goes to infinity.

These relations appear for the most part in Taylor (1921) and are well known, but the application to in situ data is often problematic. Which form of the diffusivity is the most practical to use and are the others actually equivalent? How long should one integrate the autocorrelation to obtain a convergent estimate of the diffusivity? And how are the results affected by a mean flow?

The first point was addressed by Davis (1991) and has been studied subsequently by a number of authors (e.g., Zhurbas and Oh 2003, 2004; Koszalka and LaCasce 2010; Klocker et al. 2012b). The three methods [(1), (2), and (4)] can in fact produce different results, in part because the averaging is applied at different stages. With
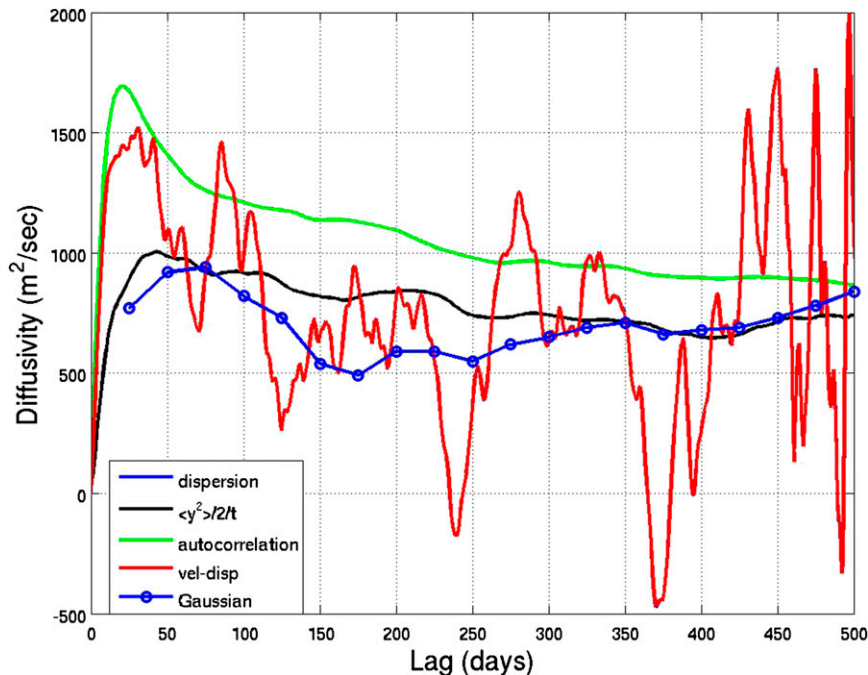
FIG. 2. The meridional diffusivity calculated in five different ways: as one-half the derivative of the dispersion [(1); blue], as the velocity–displacement correlation [(2); red], from the integral of the autocorrelation [(4); green], from the dispersion divided by 2t (black), and from fitting the displacements with a Gaussian [(8); blue with circles]. The first two curves are indistinguishable in the figure.

the dispersion equation [(1)], the time derivative is taken after averaging the squared displacements, while with the autocorrelation equation [(4)] averaging occurs prior to integration, which itself is a smoothing operation. In previous studies, one method or another is used or a combination. Zhurbas and Oh (2003), for example, recommend using the minor principal component of the diffusivity tensor obtained by combining the velocity–displacement correlation and the derivative of the dispersion.

We illustrate the results from the three methods using one set of 600 synthetic particles from the MITgcm. These were deployed on the $\gamma = 27.95$ surface at 60°S between 100° and 110°W. As seen in Fig. 2, the derivative of the dispersion and the velocity–displacement correlation yield identical results. But these estimates are also quite noisy, oscillating between -500 and $2000\,\mathrm{m^2\,s^{-1}}$. The integral of the autocorrelation yields a smoother curve, increasing to $1700\,\mathrm{m^2\,s^{-1}}$ before decreasing to a value half as large.

If the diffusivity asymptotes to a constant value, the probability density function (PDF) $p(y, t)$ of the particles' meridional displacements should, after some initial transient, evolve according to a diffusion equation (e.g., Risken 1989):

$$\frac{\partial}{\partial t}p = \kappa \frac{\partial^2}{\partial y^2}p. \tag{7}$$

Given a delta function initial condition (all particles begin at their starting latitude), the solution is Gaussian:

$$p(y) = \frac{1}{\sqrt{4\pi\kappa t}}\exp\left(-\frac{y^2}{4\kappa t}\right), \tag{8}$$

where the prefactor ensures the PDF is normalized.

The statistical moments derive from this. The mean, the first moment, is zero because the PDF is symmetric about zero. The variance, the second moment, is

$$\mathrm{var}(y) = \langle y^2 \rangle - \langle y \rangle^2 = \langle y^2 \rangle = \int_{-\infty}^{\infty} y^2 p(y)\,dy = 2\kappa t. \tag{9}$$

Thus, the diffusivity

$$\kappa_y \equiv \frac{1}{2}\frac{d}{dt}\langle y^2 \rangle = \kappa \tag{10}$$

is constant.

As seen in (9), the diffusivity can also be calculated by dividing the variance by 2t. This yields a fourth estimate
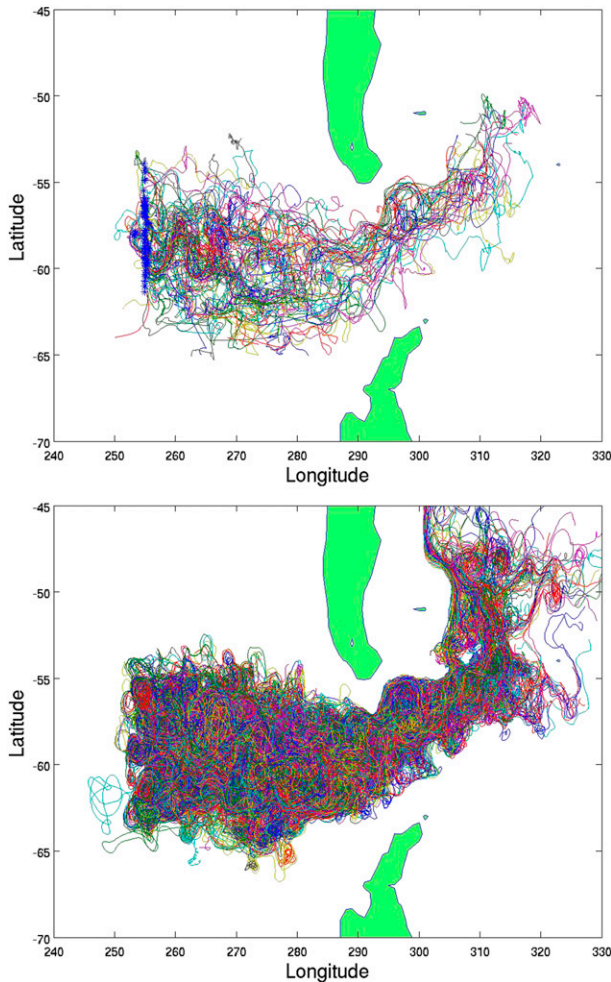
FIG. 3. (top) Trajectories of the DIMES floats and the (bottom) particles deployed in the MITgcm. The former includes the 109 floats deployed near 105°W (deployment locations are indicated by the blue asterisks), while the particles were deployed on the $\gamma =$ 27.7 surface, initially at 950-m depth.

for the diffusivity, indicated by the black curve in Fig. 2. Though less than the first three estimates initially, it asymptotes to a value similar to that derived from the integral of the autocorrelation. Note that the variance-derived estimate is not expected to hold at early times, when the spreading is ballistic (Taylor 1921), but the late behavior is consistent with that of the other measures.

There is in addition a fifth estimate in Fig. 2. This comes from fitting the meridional displacements to a Gaussian distribution [(8)] using least squares. As with the previous estimate, this assumes diffusive spreading and is thus only relevant after the initial period. The resulting diffusivity is somewhat less during the intermediate period than the variance divided by 2t. But it asymptotes to a value near $800 \, \mathrm{m^2 \, s^{-1}}$ at later times, in line with the third (autocorrelation) and fourth estimates.

The disagreement at intermediate times occurs because the PDF then is not actually Gaussian. One can test the deviation from Gaussianity using the kurtosis (the normalized fourth moment). This is three for a Gaussian, but it is larger during the intermediate period, as shown hereafter. Alternatively, one can use the Kolmogorov–Smirnov (KS) test (e.g., Press et al. 1992). This compares two PDFs by differencing their integrals—the cumulative density function (CDF). The CDF corresponding to (8) is

$$C(y) = \int_{-\infty}^{y} p(y') \, dy' = 1 - \frac{1}{2} \mathrm{erfc}\left(\frac{y}{\sqrt{4\kappa_y t}}\right), \qquad (11)$$

where erfc is the complimentary error function. The KS test assesses the probability that the maximum difference between the observed CDF and (11) can occur, given the number of degrees of freedom. Other statistical tests can also be used for testing deviations from Gaussianity (e.g., LaCasce 2005), but the KS test is perhaps the most familiar. We use the test hereafter to compare the observed meridional PDF with Gaussians with different diffusivities.

That the diffusivity reaches a maximum value before asymptoting to a smaller value, as seen in Fig. 2, is often observed. This reflects mixing suppression, in this case by the mean flow (Marshall et al. 2006; Ferrari and Nikurashin 2010; Klocker et al. 2012b; Sallée et al. 2011; Klocker et al. 2012a). The mean alters the potential vorticity (PV) gradient, permitting eddy propagation, and this in turn hinders the eddies' ability to mix properties across stream. The effect often manifests as a meandering motion, like that seen in Fig. 3. The initial meridional spreading is followed by a convergence toward the starting latitudes, and this results in a negative lobe in the autocorrelation. One must integrate past this to accurately determine the diffusivity. Not doing so, for example, by integrating to the first zero crossing of the autocorrelation, yields an overly large estimate. However, the time over which one integrates is limited because errors in the autocorrelation grow with lag (Davis 1991). The regional coverage also increases with lag, possibly violating assumptions of homogeneity. So an intermediate time is generally chosen.

To summarize, the velocity displacement [(2)] and dispersion [(1)] methods yield noisier estimates than integrating the autocorrelation [(4)]. Dividing the variance by 2t, as for a diffusive process with a constant diffusivity, yields a consistent asymptotic estimate. This approach is particularly appealing for its simplicity. However, it is important to check whether the PDFs are actually Gaussian; if not, Fickian diffusion with a constant diffusivity cannot be assumed. But if they are, fitting the
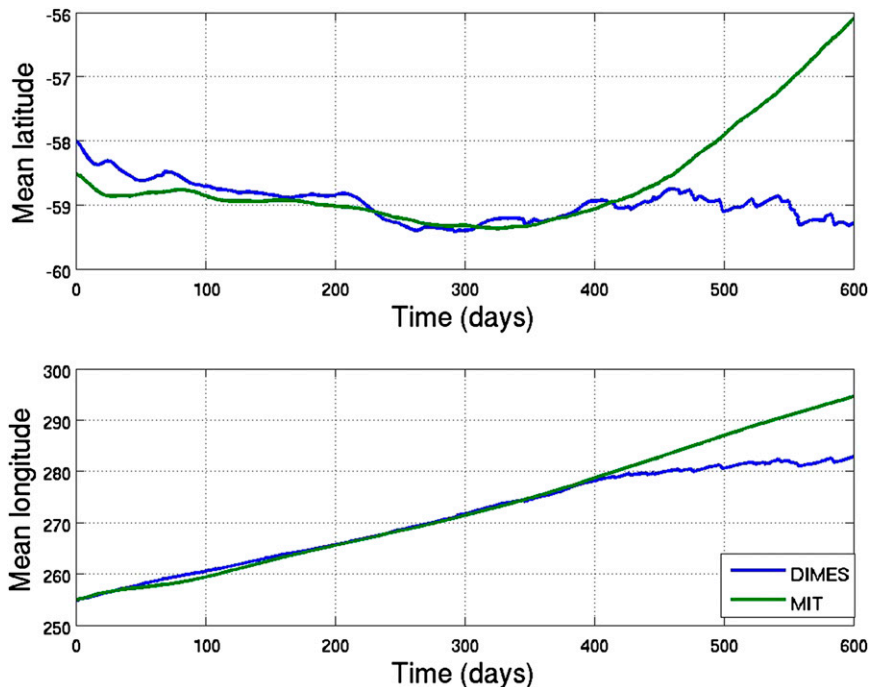
FIG. 4. Mean (top) lat and (bottom) lon of the DIMES floats (blue) and particles (green). The first moments are seen to agree well between particles and floats, prior to entering the Drake Passage at about 400 days.

displacement PDFs to a Gaussian yields an additional way of finding the diffusivity.

Hereafter, we calculate meridional diffusivities using both in situ and synthetic data from the DIMES region. Comparing the evolving PDFs to a Gaussian with a constant diffusivity allows for identifying when the spreading is diffusive and which values of the diffusivity are plausible. This offers an advantage over arbitrarily deciding when, for example, to truncate the integral of the autocorrelation.

4. Results

We first examine the DIMES floats and synthetic particles[1] launched at 105°W to obtain an estimate of the meridional diffusivity in the deployment region. Then we use the same methods to calculate diffusivities for a second set of synthetic particles launched at 60°S, between 110° and 100°W. These were used to determine the variation of κ_y with depth.

a. DIMES floats

The particles were launched in approximately the same location as the floats, but it was a question at which depth

they should be deployed because the floats did not stay on their target densities. So we compared the mean longitudinal position for the floats with those of particles deployed on 20 different density surfaces. It turned out that the result for the particles released on the $\gamma = 27.7$ surface yielded the best match (Fig. 4, bottom). Those deployed on shallower surfaces moved faster eastward while those deployed on deeper surfaces moved slower. The mean eastward displacement for both floats and particles grows nearly linearly in time. Over 400 days, the mean longitude increases by roughly 25°, corresponding to a mean velocity of about 4 cm s^{-1}. This compares well with the model mean zonal velocity of 4.2 cm s^{-1} at 950-m depth (the deployment depth of the particles).

After roughly 450 days, the floats move more slowly than the particles, implying the particle trajectories differ in and east of the Drake Passage. This is partly due to having more particles, sampling a larger area, but also to differences in the vertical motion. The density surfaces steepen drastically in the Drake Passage and the particles follow the surfaces, in some cases even surfacing. But the floats remain submerged, due in part to their compressibility behavior. As the mean flow is vertically sheared, this affects the horizontal motion. These differences in the Drake Passage further motivated our choice to focus on the region west of the Drake Passage in the present work.

---

[1] "Floats" hereafter refers to the in situ instruments, while "particles" are generated in the model simulation.
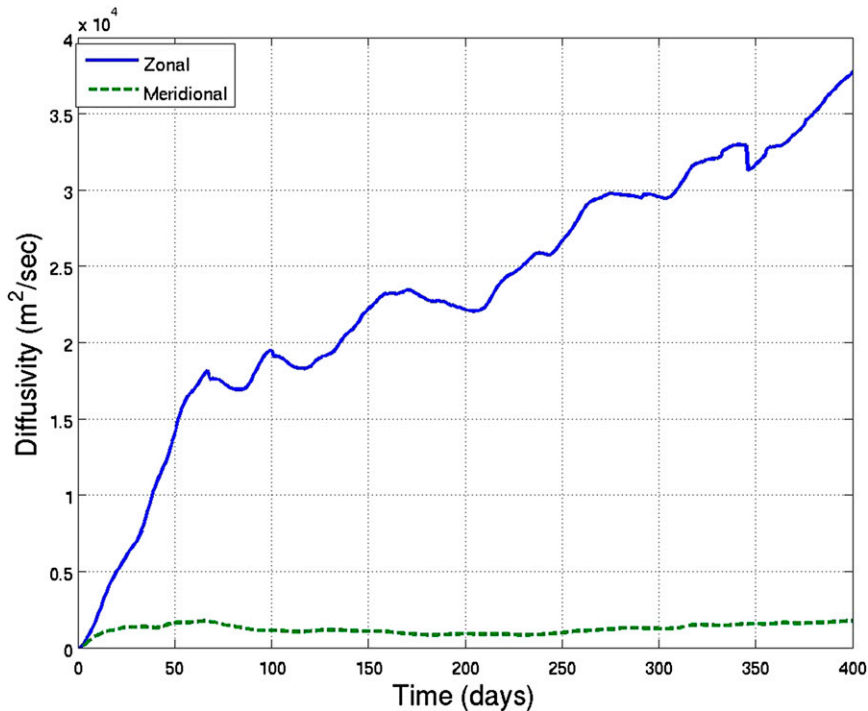
FIG. 5. Zonal (blue solid) and meridional (green dashed) diffusivities for the DIMES floats, estimated from the variance divided by $2t$. While the meridional diffusivity asymptotes to a constant value, the zonal diffusivity continues to increase, reaching large values.

The mean latitudes also compare fairly well. Both exhibit a slight southward drift over the first 300 days (Fig. 4, top). The drift is not constant in time, as the particles/floats move south during the first 25 days and again after 200 days, staying at roughly the same latitude in between. While the net displacements are small [roughly $1°$ (lat) yr^{-1}], they are large enough to affect the diffusivities, as seen below. At later times the mean latitude increases dramatically, as the floats and particles shift northward after the Drake Passage.

The mean eastward drift thus greatly exceeds the southward one, illustrating that the mean flow is largely zonal. The mean flow is also sheared with latitude, and this affects the zonal dispersion (Young and Jones 1991; Davis 1991; Bennett 2006). This is seen in Fig. 5, which shows the zonal and meridional diffusivities for the floats. These are calculated as

$$\kappa_x = \frac{\mathrm{var}(x)}{2t} \quad \text{and} \quad \kappa_y = \frac{\mathrm{var}(y)}{2t}, \qquad (12)$$

where $\mathrm{var}(x)$ and $\mathrm{var}(y)$ are the variances of the respective displacements. Note that using the variance removes the mean contribution to the diffusivity, that is, due to the drifts seen in Fig. 4.

The meridional diffusivity (the dashed curve) is bounded over this period, with a value less than $1000\,\mathrm{m}^2\,\mathrm{s}^{-1}$. The zonal diffusivity instead grows continuously, exceeding $35\,000\,\mathrm{m}^2\,\mathrm{s}^{-1}$ by 400 days. The dispersion of the float pairs (discussed in a subsequent paper) suggests the initial spreading is largely isotropic, so the asymmetry seen here probably stems from the zonal shear. Thus, we restrict our attention hereafter to the meridional diffusivity, as noted earlier. The assumption is that the actual zonal diffusivity is of similar magnitude but is difficult to extract, given the mean's contribution.

An expanded view of the meridional diffusivities is shown in Fig. 6. The float diffusivity (blue curve) increases to about $1700\,\mathrm{m}^2\,\mathrm{s}^{-1}$ before falling to a value roughly half as large. The velocity autocorrelation (not shown) has a negative lobe, which accounts for the decrease. At 250 days, when the floats begin to enter the Drake Passage, the diffusivity increases and then decreases once again.

If we calculate the diffusivity using the displacement from the initial latitude instead, we obtain the red curve. This is larger, reaching a maximum of roughly $2200\,\mathrm{m}^2\,\mathrm{s}^{-1}$. The mean drift (the only difference between the two curves) is thus large enough to alter the diffusivity.

The particle diffusivity (the green curve) behaves similarly, increasing and then decreasing, before increasing again when the particles reach the Drake Passage. The initial maximum is larger (over $2000\,\mathrm{m}^2\,\mathrm{s}^{-1}$) and
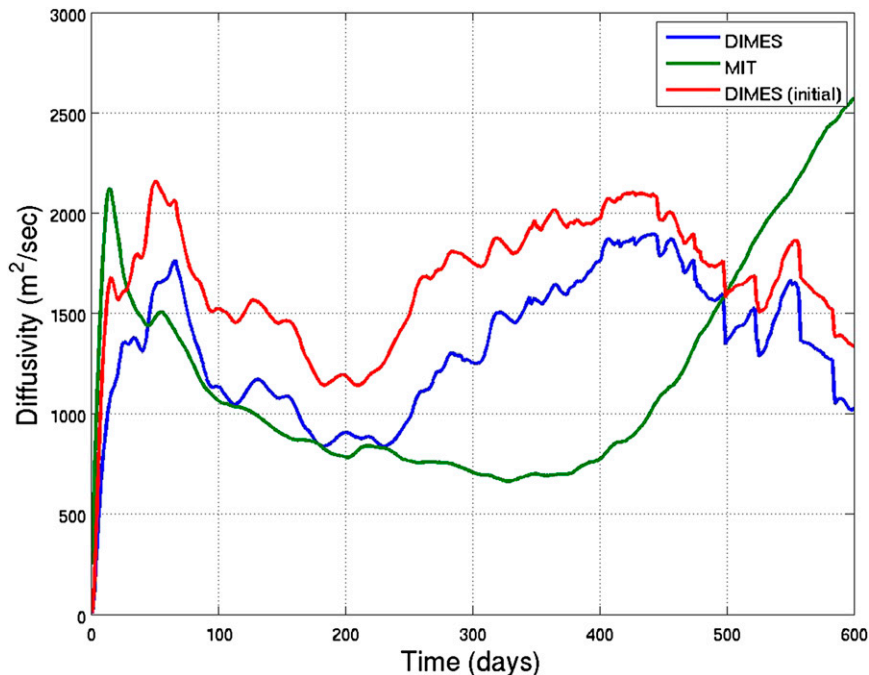
FIG. 6. The diffusivity (the meridional variance divided by 2t) for the floats (blue) and particles (green). The two estimates agree over the period 80–220 days. The float dispersion from the initial lat is somewhat larger than that about the center of mass (red).

comparable to that obtained using the displacement from the starting latitude. It also occurs earlier than the maximum in the float diffusivities. The minimum value is also less (nearer $700 \, \mathrm{m^2 \, s^{-1}}$) and this occurs after the float diffusivity is at its minimum. Nevertheless, the particle estimate agrees with the float diffusivity during the period from roughly 80–220 days.

Given these results, it is difficult to assign a single value for the diffusivity. The early maximum is one choice, but this neglects the mean flow suppression. Extracting the asymptotic value is not possible either, because the floats are entering the Drake Passage. So an intermediate value is desirable. But which one?

To decide, we examine the meridional displacement PDFs (Fig. 7). Note these are calculated with respect to the mean latitude (which is slowly decreasing; Fig. 4). At 25 days, the float PDF is non-Gaussian, being peaked and also skewed. The particle PDF is also non-Gaussian but less so (due in part to there being 7 times more particles). The PDFs thereafter become more Gaussian, but even at 100 days there are noticeable deviations. It is only at 200 days that the two distributions are plausibly Gaussian. In any case, the PDFs are clearly not Gaussian when the float diffusivity reaches its maximum at 50 days and when the particle diffusivity reaches its maximum at 25 days (Fig. 6).

At 200 days, the PDFs compare favorably to a Gaussian with a diffusivity of $800 \, \mathrm{m^2 \, s^{-1}}$. In Fig. 8, the particle PDF is compared to Gaussians with four different diffusivities. The best agreement obtains with a value of κ_y of $800 \, \mathrm{m^2 \, s^{-1}}$. The smaller diffusivities yield too narrow distributions, while $\kappa_y = 1200 \, \mathrm{m^2 \, s^{-1}}$ yields one that is too broad.

But which diffusivities are acceptable, given the statistical variations? To assess this, we use the KS test (section 3). In particular, we compare the observed distribution with the Gaussian with a chosen diffusivity at every time step. The results for the particles are shown in Fig. 9. We plot the probability p that the two PDFs are the same; if $p < 0.05$, they are different with 95% confidence.

With $\kappa_y = 200 \, \mathrm{m^2 \, s^{-1}}$, the probability is less than 0.05 during the entire first 400 days. With $\kappa_y = 400 \, \mathrm{m^2 \, s^{-1}}$, $p < 0.05$ during the first 175 days but increases thereafter. So, $\kappa_y = 400 \, \mathrm{m^2 \, s^{-1}}$ is a reasonable choice during the later period. With $\kappa_y = 800 \, \mathrm{m^2 \, s^{-1}}$, the probability exceeds the 0.05 threshold at intermediate times between 75 and 250 days. And with the largest value, $\kappa_y = 1200 \, \mathrm{m^2 \, s^{-1}}$, the probability is large during the initial phase from roughly 30 to 130 days.

The preferred value is that which applies during the intermediate period, as the early phase is affected by mean flow suppression, and in the later period the particles are
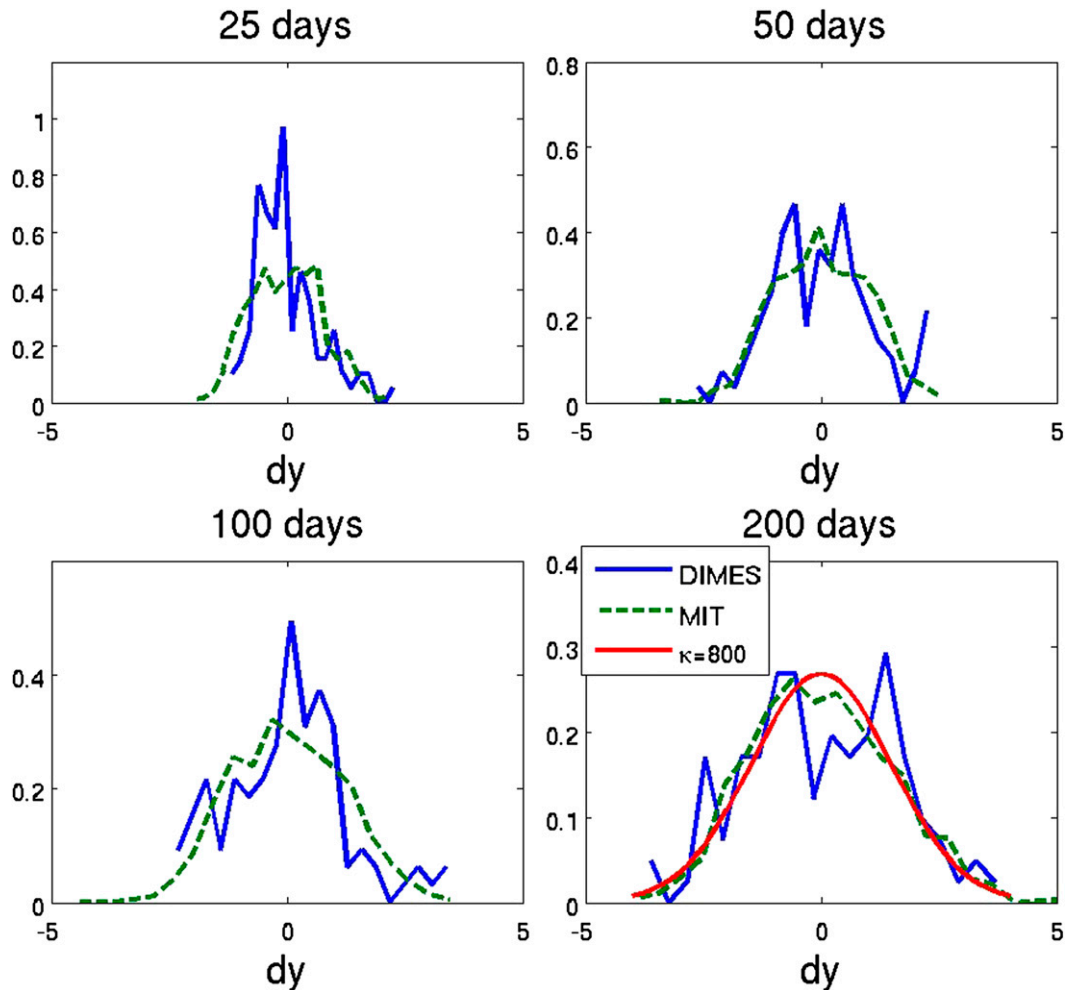
FIG. 7. Meridional displacement PDFs for the DIMES floats and MIT particles at (top left) 25, (top right) 50, (bottom left) 100, and (bottom right) 200 days. A Gaussian with a diffusivity of $800\,\mathrm{m^2\,s^{-1}}$ is shown for comparison (bottom right).

entering the Drake Passage. Nevertheless, the figure illustrates that a range of values is possible. A reasonable estimate is $800 \pm 200\,\mathrm{m^2\,s^{-1}}$.

The corresponding results for the floats are shown in Fig. 10. Again, we can rule out $\kappa_y = 200\,\mathrm{m^2\,s^{-1}}$ as being too low and $\kappa_y = 1200\,\mathrm{m^2\,s^{-1}}$ as too high. The best value is also $\kappa_y = 800\,\mathrm{m^2\,s^{-1}}$, which yields the largest probabilities during the period 80–220 days. So as with the floats, a reasonable estimate is $800 \pm 200\,\mathrm{m^2\,s^{-1}}$.

As noted, there are roughly 7 times as many particles as floats. But the number determines the degrees of freedom, which in turn affect the probability in the KS test. For the floats, we took the degrees of freedom to be equal to the number of floats. For the particles, we divided the number by 5 because the particles were deployed in tighter clusters. Using a different value alters the magnitude of the probability but not the qualitative behavior.

So, the results are well captured by Fig. 7 (bottom right). After 200 days, the meridional displacement distributions for the floats and particles are similar. The particles have a smoother PDF, as there are more of them. But within the errors (as assessed by the KS test), both are statistically indistinguishable from a Gaussian distribution with a diffusivity of $800\,\mathrm{m^2\,s^{-1}}$.

b. Variation with depth

As noted, the reason the DIMES floats were deployed on two density surfaces was to detect vertical variations in the diffusivity. Owing to the floats' loss of buoyancy, this could not easily be assessed with the in situ data. But as the MITgcm yields a diffusivity that is identical within the errors to the floats', we can use the model to study this.

Such variations have been seen previously. Abernathey et al. (2010) diagnosed a subsurface maximum in diffusivity
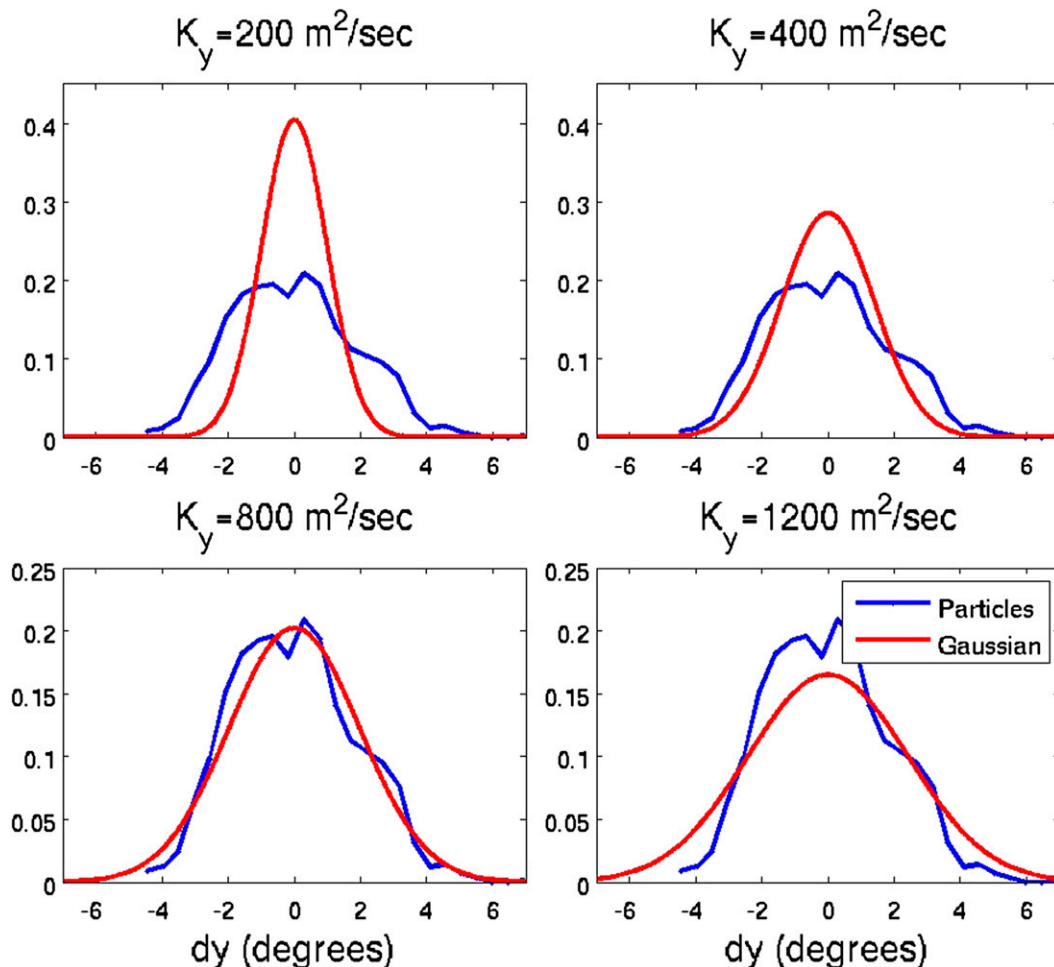
FIG. 8. Meridional displacement PDFs at 1 yr for the particles, with Gaussian distributions with four values of the diffusivity.

using synthetic tracer in an eddy-permitting state estimate [Southern Ocean State Estimation (SOSE)]; while the diffusivity was $500 \, \mathrm{m}^2 \, \mathrm{s}^{-1}$ near the surface, it increased to $2000 \, \mathrm{m}^2 \, \mathrm{s}^{-1}$ at roughly 1500-m depth in the core of the ACC. Klocker et al. (2012b) obtained a similar result using a 3D velocity field reconstructed from satellite data, with the diffusivity increasing from $600 \, \mathrm{m}^2 \, \mathrm{s}^{-1}$ at the surface to over $1000 \, \mathrm{m}^2 \, \mathrm{s}^{-1}$ at 1500-m depth. Their estimates moreover derive both from tracer and particle dispersion. Likewise, Tulloch et al. (2013, manuscript submitted to *J. Phys. Oceanogr.*) found the diffusivities increased from around $500 \, \mathrm{m}^2 \, \mathrm{s}^{-1}$ above 1000 m to nearly $1000 \, \mathrm{m}^2 \, \mathrm{s}^{-1}$ at 2000 m, using tracer in the MITgcm.

We are using the same model, so the subsurface maximum evidently exists; the question is whether we can detect it using particles and the present methods. To this end, we employ a second set of particles, deployed at 60°S, between 110° and 100°W, on 20 different γ surfaces. For each of the 20 sets of particles, we calculated diffusivities

from the meridional displacements using the variance divided by 2t and by least squares fits of the displacement PDFs (with the mean displacement removed) to a Gaussian. The values are reported as a function of the initial depth of the γ surface on which the particles were released.

Though this calculation is straightforward, it is hindered by two effects in the DIMES region. At the shallower levels, the particles are advected rapidly toward the Drake Passage, shortening the "diffusive period" experienced by the particles. Consider the diffusivities at 370-m depth shown in the upper panel of Fig. 11. These peak after 10 days and decrease thereafter. The two methods moreover produce comparable estimates after 100 days. But at 200 days the diffusivities increase again, as the particles enter the Drake Passage and veer north.

The latter increase can be avoided by excluding all particle positions east of 70°W. Doing this yields the estimate shown by the dashed curve (also calculated from
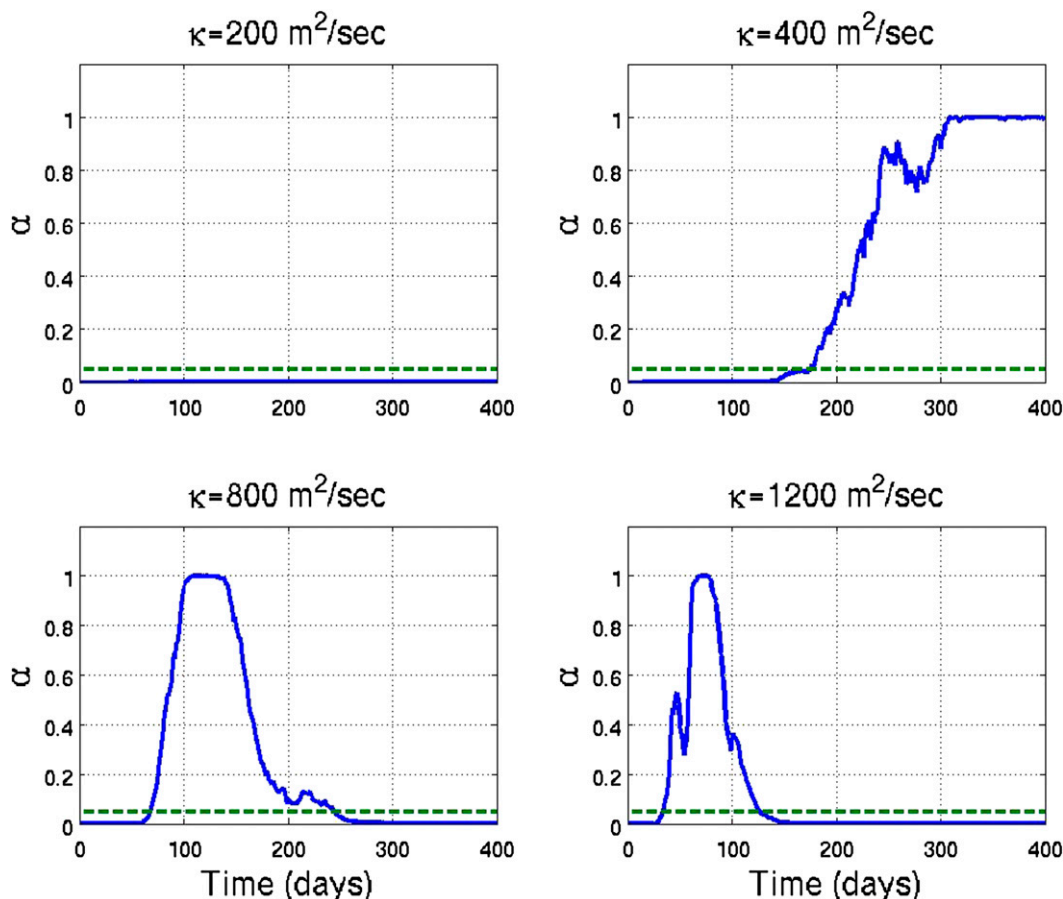
FIG. 9. The probability, from the KS test, that the particle displacement PDF is the same as a Gaussian with the diffusivity shown as a function of time. Probabilities less than 0.05 (dashed) indicate that they are different with 95% confidence. The results suggest $\kappa = 800 \, \mathrm{m}^2 \, \mathrm{s}^{-1}$ yields the best match during the intermediate period.

the variance). After 200 days, this diffusivity continues to decrease (because the mean flow converges as it approaches the Drake Passage). As such, it is not clear what the true asymptotic diffusivity at 370 m is.

In contrast, most of the particles at 1500-m depth (Fig. 11, bottom) do not reach the Drake Passage during the first 600 days. So the diffusivity obtained excluding particles east of 70°W is nearly the same as that for the full set. But unlike at 370 m, the two estimates do not agree as well, particularly at around 200 days. Then the variance-based estimate is near $750 \, \mathrm{m}^2 \, \mathrm{s}^{-1}$, while the one based on the Gaussian fit dips to $400 \, \mathrm{m}^2 \, \mathrm{s}^{-1}$.

The reason is that the displacement PDFs during the intermediate period are not Gaussian. Consider the kurtoses, shown in Fig. 12. These are large during the first 25 days, at both 370 and 1500 m, that is, when the distributions are spiky (Fig. 7). They decrease thereafter. At 370 m, the value is between 3 and 4 until day 200 when it settles to around 3. This is when the Gaussian- and variance-derived diffusivities agree well (Fig. 11), before

the particles enter the Drake Passage. The kurtosis at 1500 m on the other hand is near 4 at 200 days and falls to 3 only after 300 days. So when the Gaussian- and variance- derived diffusivities differ, the kurtosis is elevated. Consistently, the PDF at day 200 is somewhat peaked, with extended wings (Fig. 7). So the variance differs from that of the best-fit Gaussian.

Thus, the diffusivities at the shallower levels are affected by the particles entering the Drake Passage while those at deeper levels experience a delay before settling into the diffusive regime. With this in mind, we examine the diffusivities as a function of depth at various times. For this we use the estimate derived from fitting the PDF to a Gaussian and exclude all particle positions east of 70°W. The diffusivities at 0.5, 1, and 1.5 yr are shown in Fig. 13.

At half a year, the diffusivities are greatest near the surface, with values over $600 \, \mathrm{m}^2 \, \mathrm{s}^{-1}$. They fall abruptly at 1000 m and are in the range 400–$600 \, \mathrm{m}^2 \, \mathrm{s}^{-1}$ below that. At 1 yr, the shallower diffusivities have decreased, but the
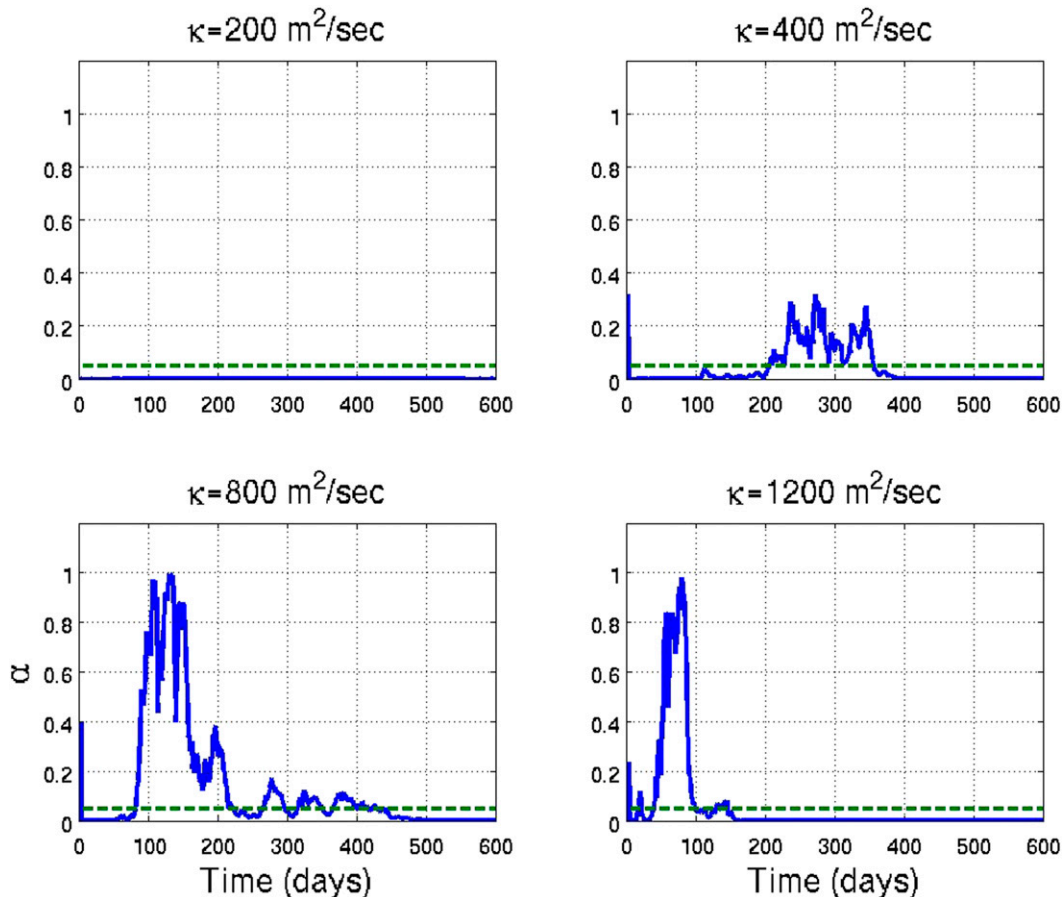
FIG. 10. As in Fig. 9, but for the DIMES floats.

deeper ones have increased. They reach values of about $900\,\mathrm{m}^2\,\mathrm{s}^{-1}$ from 1400 to 2200 m and are less above and below. At 1.5 yr, the diffusivities below 1000 m are consistent, but the shallower diffusivities continue to decrease.

So the diffusivities above 1000 m are, perhaps, not to be trusted. Their decrease reflects the convergence of the mean flow (this effect would presumably be absent when using cross-stream displacements, rather than meridional distance). The deeper diffusivities are not so affected and appear to converge after about 1 yr. These indicate a middepth maximum between roughly 1500 and 2000-m depth, with values that are $500\,\mathrm{m}^2\,\mathrm{s}^{-1}$ larger than at 1000-m depth.

One may have noticed that the diffusivity at 1000 m is somewhat less than the $800\,\mathrm{m}^2\,\mathrm{s}^{-1}$ obtained in section 4a. The reason is that this set of particles was deployed along a latitude line (60°S) rather than on a longitude line, as in DIMES. The floats sample the mixing occurring north of 60°S as well, and this yields a somewhat larger value.

Similar diffusivities were obtained by Tulloch et al. (2013, manuscript submitted to *J. Phys. Oceanogr.*) using a passive tracer with this model (see their Fig. 10).

Their diffusivities increased from about $500\,\mathrm{m}^2\,\mathrm{s}^{-1}$ at 900 m to $900\,\mathrm{m}^2\,\mathrm{s}^{-1}$ at 2000 m and decreased again at deeper levels. The advecting velocities are the same, but the method of calculation is quite different (theirs comes from differencing the dispersion at 100 and 400 days). The present results suggest those choices are reasonable; the non-Gaussian initial period is largely over by 100 days, and the deeper diffusivities converge by 1 yr. Their estimates are the same as ours, within the errors.

5. Summary and discussion

We have calculated isopycnal diffusivities using floats deployed in the DIMES experiment and particles advected in a high-resolution MITgcm simulation of the eastern Pacific sector of the Southern Ocean. We focused on the meridional diffusivity, as this is less affected by the large-scale shear associated with the ACC. The floats span a range of densities, having encountered problems maintaining buoyancy, and we took the entire set together for the present work. The particles that displayed the most similar mean drifts were those on the $\gamma = 27.7$ neutral
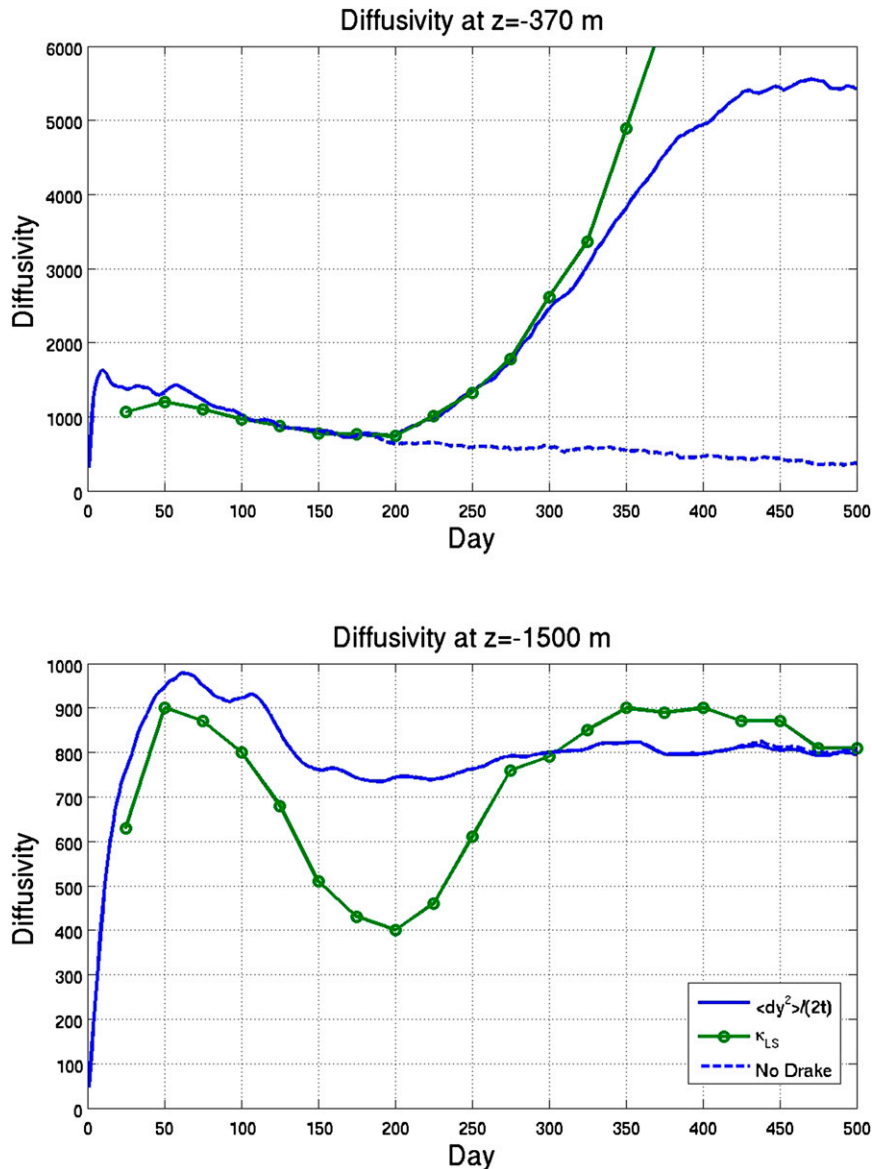
FIG. 11. The diffusivities as a function of time for the particles deployed at 60°S at (top) 370- and (bottom) 1500-m depth. The diffusivities are estimated from the meridional variance (blue solid) and the best-fit Gaussian (green with circles). The diffusivities obtained when excluding particles east of 70°W are indicated by the blue dashed curves.

density surface, deployed at 950-m depth. The float and model diffusivities are equivalent within the errors, with a value of $800 \pm 200 \, \mathrm{m^2 \, s^{-1}}$.

We then assessed the diffusivity's dependence on depth, using a second set of particles deployed at 60°S. Obtaining the diffusivities above 1000 m was hindered by the particles reaching the Drake Passage, but this was not the case below 1000 m. The results suggest the diffusivity increases from a value near $500 \, \mathrm{m^2 \, s^{-1}}$ at 1000 m to roughly $900 \, \mathrm{m^2 \, s^{-1}}$ between 1500 and 2000 m before decreasing again at greater depths. This is in line with

tracer-based estimates using the MITgcm (Tulloch et al. 2013, manuscript submitted to *J. Phys. Oceanogr.*).

The subsurface maximum in diffusivity was found previously by Smith and Marshall (2009), Abernathey et al. (2010), Lu and Speer (2010), and Tulloch et al. (2013, manuscript submitted to *J. Phys. Oceanogr.*) using tracer in models and by Klocker et al. (2012b) with tracer and particles advected by altimeter-derived velocities (projected downward assuming an equivalent barotropic profile). Their diffusivities are comparable to ours, peaking at 1500–2000 m. Most of the DIMES floats
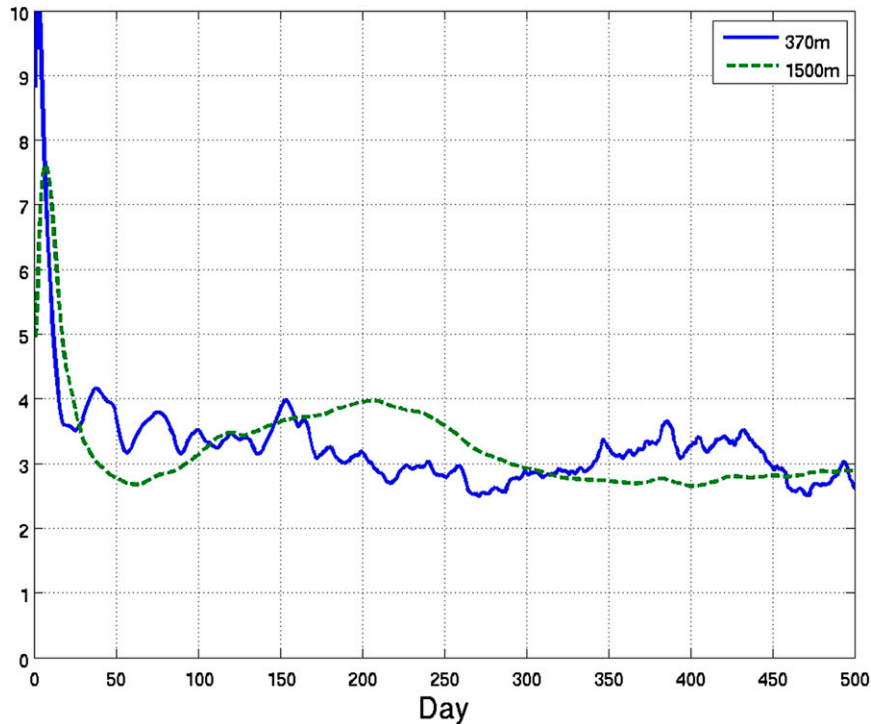
FIG. 12. The displacement kurtoses for the particles at (blue solid) 370- and (green dashed) 1500-m depth.

were deployed above this maximum, but D. Balwada et al. (2013, unpublished manuscript) see hints of a maximum by analyzing subsets of the float data. Tulloch et al. (2013, manuscript submitted to *J. Phys. Oceanogr.*) show that the subsurface maximum does indeed coincide with a critical layer in this simulation.

While this is the first estimate of the subsurface diffusivity in the ACC west of the Drake Passage derived from continuously tracked floats, others have inferred diffusivities using different methods. Faure and Speer (2013) inferred a value of $\kappa_y = 300 \pm 100 \, \mathrm{m^2 \, s^{-1}}$ in the deep interior region of the southeastern South Pacific Ocean from an advective–diffusive formulation. This is consistent with having a smaller diffusivity outside the core of the deep ACC maximum. Naveira Garabato et al. (2007) obtained relatively large diffusivities ($\kappa_y = 1840 \pm 440 \, \mathrm{m^2 \, s^{-1}}$) at middepths east of the Drake Passage, but found smaller values near the core of the ACC ($360 \pm 330 \, \mathrm{m^2 \, s^{-1}}$). Other estimates suggest subsurface values in the lower range in other regions of the Southern Ocean: 300–$600 \, \mathrm{m^2 \, s^{-1}}$ at 900-m depth (Gille 2003) and 100–$500 \, \mathrm{m^2 \, s^{-1}}$ (Phillips and Rintoul 2000) and $300 \pm 150 \, \mathrm{m^2 \, s^{-1}}$ in circumpolar estimates from the inversion of tracer fields at middepth (Zika et al. 2009). The differences stem in part from using different methods, but also reflect regional variations in the vertical and horizontal mixing in the Southern Ocean.

One of our goals was to assess different ways of calculating the diffusivity from Lagrangian data. Typically this is done using the time derivative of the dispersion, the velocity–displacement correlation or the integral of the velocity autocorrelation (Davis 1991; Zhurbas and Oh 2003; LaCasce 2008). We find that two alternate approaches—dividing the variance by $2t$ or fitting the displacement PDFs with a Gaussian function—are straightforward to calculate and are robust. Comparing these two estimates is also instructive, as it reveals when the PDFs are non-Gaussian. In the DIMES region, the initial dispersion is non-Gaussian and hence not diffusive. Better estimates are obtained when the distributions are normal, and this can be assessed using the Kolmogorov–Smirnov test. Such an approach also reveals what ranges of diffusivities are plausible.

A striking result is how long it takes for the diffusivities to converge. At the shallower levels (above 1000 m), the diffusivities fail to converge before the particles have left the region. At the deeper levels (below 1000 m), convergence takes a full year. So the diffusivities must be integrated to times that are substantially longer than the integral time, which is on the order of days. This has serious implications for regional diffusivity estimates, as the particles cover a large area in 1 yr. One option, when using synthetic particles, is to extract the velocities from a given region and then impose zonal periodicity on the
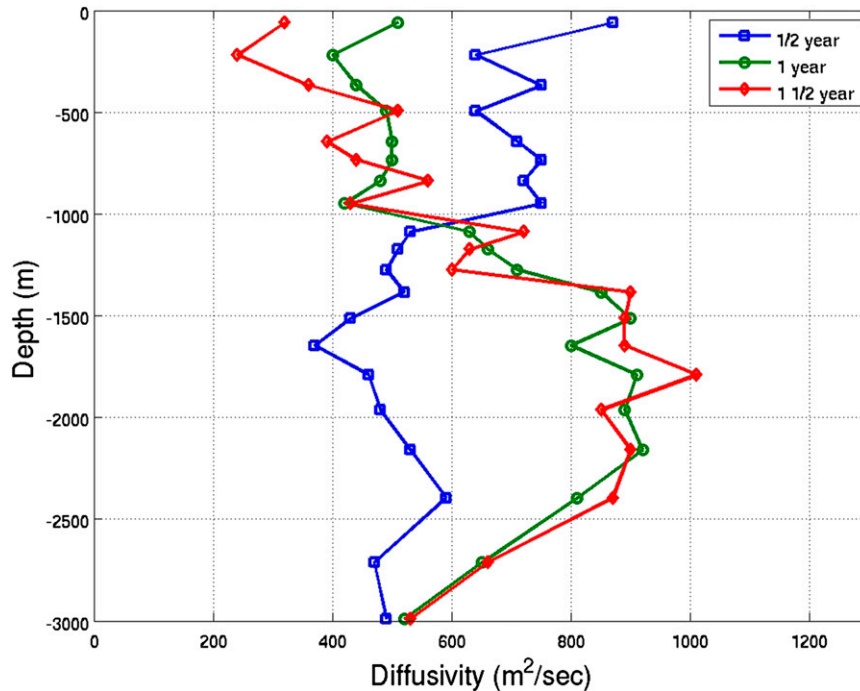
FIG. 13. The diffusivities as a function of depth for the 60°S particles at three different times.
The estimates were made using the Gaussian fit method.

advecting field, as done by Klocker et al. (2012b) for the DIMES region. Their result (at the surface) is like what we observe after a half year of dispersion.

For simplicity, and because of the importance of the cross-stream component of lateral mixing in the ACC, we focused on the meridional diffusivity west of the Drake Passage. We were not able to obtain estimates in the Scotia Sea, where the mean flow in part veers to the north off the Patagonian shelf. Analyzing mixing in the Scotia Sea remains a challenge due to the rapid transit across the region and the necessity of using a true cross-stream component to determine exchange.

REFERENCES

Abernathey, R., J. Marshall, M. Mazloff, and E. Shuckburgh, 2010: Critical layer enhancement of mesoscale eddy stirring in the Southern Ocean. *J. Phys. Oceanogr.,* **40,** 170–184.

Bennett, A. F., 2006: *Lagrangian Fluid Dynamics.* Cambridge Monographs on Mechanics Series, Cambridge University Press, 286 pp.

Davis, R., 1991: Observing the general circulation with floats. *Deep-Sea Res.,* **38A,** S531–S571.

Faure, V., and K. Speer, 2013: Deep circulation in the eastern South Pacific Ocean. *J. Mar. Res.,* **70,** 748–778.

Ferrari, R., and M. Nikurashin, 2010: Suppression of eddy diffusivity across jets in the Southern Ocean. *J. Phys. Oceanogr.,* **40,** 1501–1519.

Freeland, H., P. Rhines, and T. Rossby, 1975: Statistical observations of the trajectories of neutrally buoyant floats in the North Atlantic. *J. Mar. Res.,* **33,** 383–404.

Gille, S., 2003: Float observations of the Southern Ocean. Part II: Eddy fluxes. *J. Phys. Oceanogr.,* **33,** 1182–1196.

Green, J. S. A., 1970: Transfer properties of the large-scale eddies and the general circulation of the atmosphere. *Quart. J. Roy. Meteor. Soc.,* **96,** 157–185.

Griffies, S. M., 2004: *Fundamentals of Ocean Climate Models.* 1st ed. Princeton University Press, 496 pp.

Haller, G., and G. Yuan, 2000: Lagrangian coherent structures and mixing in two-dimensional turbulence. *Physica D,* **147,** 352–370.

Klocker, A., R. Ferrari, and J. H. LaCasce, 2012a: Estimating suppression of eddy mixing by mean flows. *J. Phys. Oceanogr.,* **42,** 1566–1576.

——, ——, ——, and S. T. Merrifield, 2012b: Reconciling float-based and tracer-based estimates of eddy diffusivities. *J. Mar. Res.,* **70,** 569–602.

Koszalka, I., and J. H. LaCasce, 2010: Lagrangian analysis by clustering. *Ocean Dyn.,* **60,** 957–972.

LaCasce, J. H., 2005: On the Eulerian and Lagrangian velocity distributions in the North Atlantic. *J. Phys. Oceanogr.,* **35,** 2327–2336.

——, 2008: Statistics from Lagrangian observations. *Prog. Oceanogr.,* **77,** 1–29.

Ledwell, J. R., A. J. Watson, and C. S. Law, 1998: Mixing of a tracer in a pycnocline. *J. Geophys. Res.,* **103** (C10), 21 499–21 529.

——, L. C. St. Laurent, J. B. Girton, and J. M. Toole, 2011: Diapycnal mixing in the Antarctic Circumpolar Current. *J. Phys. Oceanogr.,* **41,** 241–246.

Lu, J., and K. Speer, 2010: Topography, jets, and eddy mixing in the Southern Ocean. *J. Mar. Res.,* **68,** 479–502.

Lumpkin, R., and M. Pazos, 2007: Measuring surface currents with surface velocity program drifters: The instruments, its data and some recent results. *Lagrangian Analysis and Prediction of Coastal and Ocean Dynamics,* A. Griffa et al., Eds., Cambridge University Press, 39–67.

Marshall, J., A. Adcroft, C. Hill, L. Perelman, and C. Heisey, 1997: A finite-volume, incompressible Navier Stokes model for studies of the ocean on parallel computers. *J. Geophys. Res.,* **102** (C3), 5753–5766.

——, E. Shuckburgh, H. Jones, and C. Hill, 2006: Estimates and implications of surface eddy diffusivity in the Southern Ocean derived from tracer transport. *J. Phys. Oceanogr.,* **36,** 1806–1821.

Naveira Garabato, A. C., D. P. Stevens, A. J. Watson, and W. Roether, 2007: Short-circuiting of the overturning circulation in the Antarctic Circumpolar Current. *Nature,* **447,** 194–197.

Owens, W. B., 1991: A statistical description of the mean circulation and eddy variability in the northwestern Atlantic using SOFAR floats. *Prog. Oceanogr.,* **28,** 257–303.

Phillips, H. E., and S. R. Rintoul, 2000: Eddy variability and energetics from direct current measurements in the Antarctic Circumpolar Current south of Australia. *J. Phys. Oceanogr.,* **30,** 3050–3076.

Plumb, R. A., and J. D. Mahlman, 1987: The zonally averaged transport characteristics of the GFDL general circulation/ transport model. *J. Atmos. Sci.,* **44,** 298–327.

Press, W. H., S. A. Teukolshy, W. T. Vetterling, and B. P. Flannery, 1992: *Numerical Recipes in FORTRAN: The Art of Scientific Computing.* Cambridge University Press, 963 pp.

Risken, H., 1989: *The Fokker–Planck Equation: Methods of Solution and Applications.* Springer Series in Synergetics, Vol. 18, Springer, 474 pp.

Rupolo, V., 2007: A Lagrangian-based approach for determining trajectories taxonomy and turbulence regimes. *J. Phys. Oceanogr.,* **37,** 1584–1609.

Sallée, J. B., K. Speer, R. Morrow, and R. Lumpkin, 2008: An estimate of Lagrangian eddy statistics and diffusion in the mixed layer of the Southern Ocean. *J. Mar. Res.,* **66,** 441–463.

——, ——, and S. R. Rintoul, 2011: Mean-flow and topographic control on surface eddy-mixing in the Southern Ocean. *J. Mar. Res.,* **69,** 4–6.

Smith, K. S., and J. Marshall, 2009: Evidence for enhanced eddy mixing at middepth in the Southern Ocean. *J. Phys. Oceanogr.,* **39,** 50–69.

St. Laurent, L. C., A. C. N. Garabato, J. R. Ledwell, A. M. Thurnherr, J. M. Toole, and A. J. Watson, 2012: Turbulence and diapycnal mixing in Drake Passage. *J. Phys. Oceanogr.,* **42,** 2143–2152.

Swallow, J., 1971: The Aries Current measurements in the western North Atlantic. *Philos. Trans. Roy. Soc. London,* **270,** 451–460.

——, and L. Worthington, 1957: Measurements of deep currents in the western North Atlantic. *Nature,* **179,** 1183–1184.

Taylor, G. I., 1921: Diffusion by continuous movements. *Proc. London Math. Soc.,* **20,** 196–211.

Wiggins, S., 2005: The dynamical systems approach to Lagrangian transport in oceanic flows. *Annu. Rev. Fluid Mech.,* **37,** 295–328.

Young, W. R., and S. Jones, 1991: Shear dispersion. *Phys. Fluids,* **3,** 1087–1101.

Zhurbas, V., and I. S. Oh, 2003: Lateral diffusivity and Lagrangian scales in the Pacific Ocean as derived from drifter data. *J. Geophys. Res.,* **108,** 3141, doi:10.1029/2002JC001596.

——, and ——, 2004: Drifter-derived maps of lateral diffusivity in the Pacific and Atlantic Oceans in relation to surface circulation patterns. *J. Geophys. Res.,* **109,** C05015, doi:10.1029/ 2003JC002241.

Zika, J. D., B. M. Sloyan, and T. J. McDougall, 2009: Diagnosing the Southern Ocean overturning from tracer fields. *J. Phys. Oceanogr.,* **39,** 2926–2940.